

# Controlling the Electronic, Structural, and Optical Properties of Novel MgTiO<sub>3</sub>/LaNiO<sub>3</sub> Nanostructured Films for Enhanced Optoelectronic Devices

T. M. Mazzo,<sup>†</sup> L. R. Macario,<sup>‡</sup> L. F. Gorup,<sup>§</sup> V. Bouquet,<sup>||</sup> S. Députier,<sup>||</sup> S. Ollivier,<sup>||</sup> M. Guilloux-Viry,<sup>||</sup> A. R. Albuquerque,<sup>⊥</sup> J. R. Sambrano,<sup>#</sup> F. A. La Porta,<sup>\*,∇</sup> and E. Longo<sup>‡</sup>

<sup>†</sup>Institute of Marine Sciences, Federal University of São Paulo (UNIFESP), P. O. Box 11070-100, Santos, São Paulo 11015-020, Brazil

<sup>‡</sup>INCTMN, CDMF, Universidade Federal de São Carlos (UFSCar), Rod. Washington Luis km 235, CP 676, São Carlos, São Paulo 13565-905, Brazil

<sup>§</sup>FACET-Department of Chemistry, Federal University of Grande Dourados, Dourados, Mato Grosso do Sul 79804-970, Brasil

<sup>||</sup>Institut des Sciences Chimiques de Rennes, UMR 6226 CNRS, Université de Rennes, Campus de Beaulieu, 35042 Rennes, France

<sup>⊥</sup>Instituto de Química, Universidade Federal do Rio Grande do Norte (UFRN), 3000, Natal, Rio Grande do Norte 59078-970, Brazil

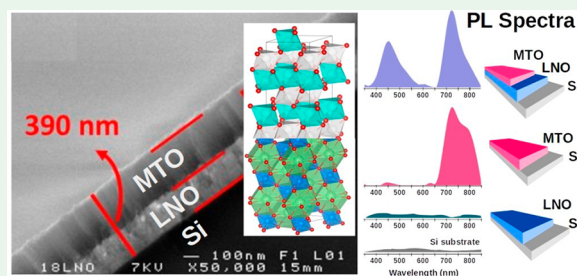
<sup>#</sup>Modeling and Molecular Simulations Group, São Paulo State University (UNESP), Bauru, São Paulo 17033-360, Brazil

<sup>∇</sup>Laboratory of Nanotechnology and Computational Chemistry, Federal Technological University of Paraná (UTFPR), Londrina, Paraná 86036-370, Brazil

## S Supporting Information

**ABSTRACT:** This study systematically investigated the electronic, structural, and optical properties of MgTiO<sub>3</sub> (MTO), LaNiO<sub>3</sub> (LNO), and MgTiO<sub>3</sub>/LaNiO<sub>3</sub> (MTO/LNO) nanostructured films grown on Si(100) substrates by the pulsed laser deposition method. The structural characterizations obtained by X-ray diffraction revealed a preferred (003) orientation for the MTO film, while the LNO film was polycrystalline. The diffraction peaks corresponded to a rhombohedral structure, which was confirmed by micro-Raman spectroscopy for both nanostructured films. The MTO/LNO heterostructure was polycrystalline and exhibited the diffraction peaks of both the MTO and the LNO phases. Additionally, the results revealed that the LNO films did not have a significant photoluminescence (PL) emission, while an intense broad infrared luminescence centered at 724 nm appeared for the MTO nanostructured film. Surprisingly, for the MTO/LNO heterostructure, the PL emission profile exhibited a dual-color emission with an intense broad luminescence in the blue region (maximum centered at 454 nm) and an intense near-infrared emission (maximum centered at 754 nm), respectively, mainly because of the effect of interface defects, which induced a significant change in the PL behavior. Therefore, our experimental results correlated with the theoretical simulations based on the periodic density functional theory formalism and contributed to a deeper understanding of the charge/energy transfer processes occurring in the MTO/LNO/Si interfaces, and toward the exploitation of the close relationship between the structure and properties of these new functional materials.

**KEYWORDS:** perovskites, thin films, pulsed laser deposition method, optical properties, DFT calculations



## 1. INTRODUCTION

In practice, the development of broadband communications, the increasing demand for light-emitting devices for displays and communication systems operating at microwave frequencies, electroluminescence, and the continuing miniaturization of circuitry systems have motivated the rapid development of highly dielectric materials with active optical properties. Moreover, it has been shown that controlling the growth of high-quality thin films not only allows for the fabrication of the most complex functional materials on scale but also provides a

form that is compatible with a wide variety of electronic and optical devices, which could give rise to new and fascinating behaviors at the nanoscale.<sup>1–3</sup>

In this context, significant advances in the pulsed laser deposition (PLD) method, and particularly over the most recent decades, provided a more versatile and innovative way toward

**Received:** November 21, 2018

**Accepted:** March 20, 2019

**Published:** March 20, 2019



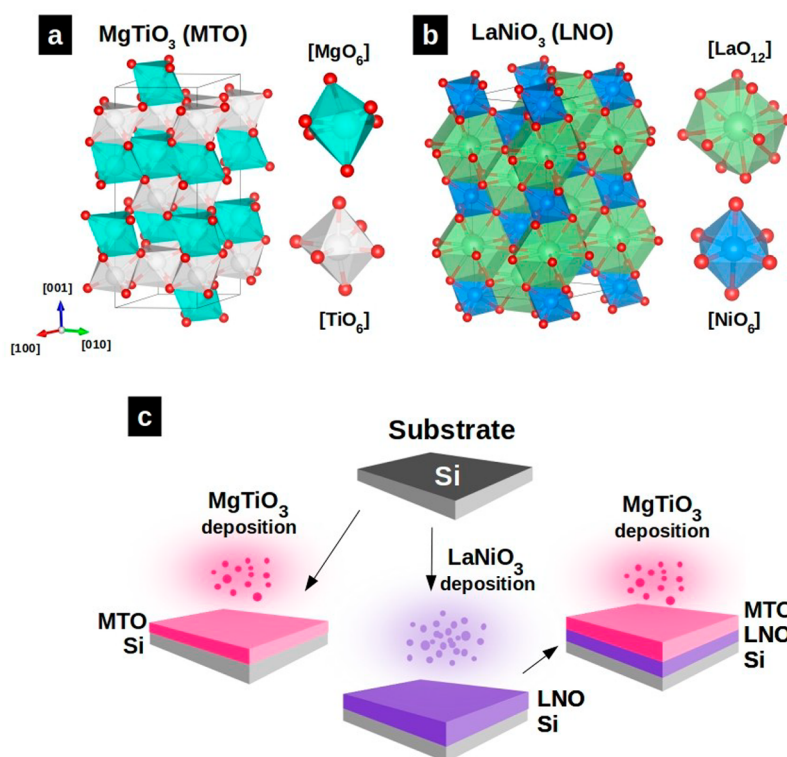


**Figure 1.** Representation of (a) MTO and (b) LNO unit cells oriented in the same direction and their metal–oxygen polyhedra. (c) Schemes illustration of the PLD process of the LNO/Si MTO/Si and MTO/LNO/Si thin films prepared by PLD technique.

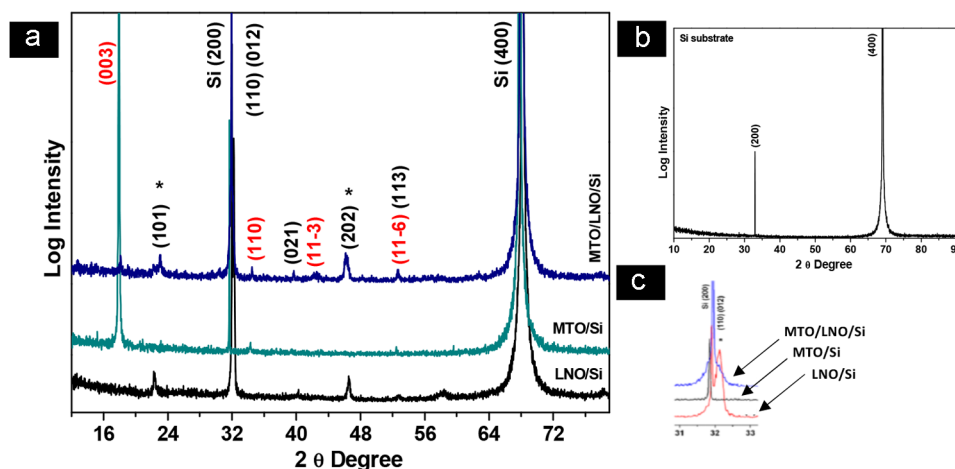


**Figure 2.** XRD patterns of (a) LNO/Si, MTO/Si and MTO/LNO/Si thin films; (b) Si(100) substrate and (c) zoom of the  $\theta$ – $2\theta$  degree.

developing high-quality thin films with entirely new physical properties.<sup>3–6</sup> This technique has been widely applied to thin film growth based on perovskite oxide materials,<sup>7–9</sup> mainly because of the sizable technological interest in these materials and their remarkable record of developing widespread applications for these novel functional materials. With rapid breakthroughs in the deposition techniques, many recent studies have focused on the development of heterojunctions from two types of perovskite oxides to build artificial superlattices for highly innovative technological applications.<sup>10–12</sup>

Among perovskite oxides, magnesium titanate (MgTiO<sub>3</sub>) (MTO) and lanthanum nickelate (LaNiO<sub>3</sub>) (LNO) have attracted large technological interest over recent years, mainly because of their extraordinary physical and chemical properties that make them promising candidates for a wide range of

technological applications such as optoelectronic devices.<sup>13–16</sup> Thus, there is continuous technological interest in using MTO and LNO materials in the form of nanostructured films for easier integration into microelectronic devices.<sup>17</sup> Considering recent research trends in the field of thin films, beyond their role in fundamental research, these novel functional materials and their well-designed heterostructures can, in principle, offer an exciting platform to develop perovskite oxide-based devices and thus lead to the development of advanced applications in the future. However, to establish their contributions toward a fundamental understanding of the mechanism responsible for modulating the optical and electronic properties of these films at the nanoscale, it is still necessary to understand how complex interface defects behave under excitation.

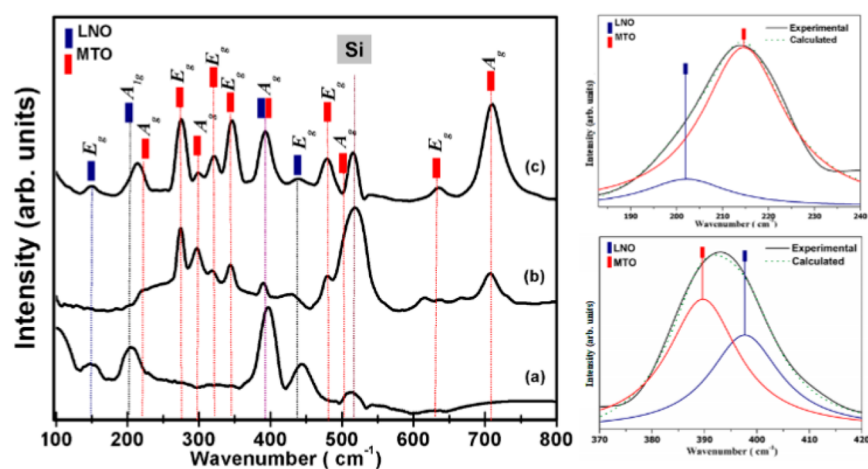


**Figure 3.** MR spectra of (a) LNO/Si, (b) MTO/Si, and (c) MTO/LNO/Si thin films.

In this work, we report a combined experimental–computational investigation on the electronic, structural, and optical properties of LNO, MTO, and MTO/LNO nanostructured films grown on a Si(100) substrate using the PLD method for the first time, as illustrated in Figure 1. All these thin films were characterized by X-ray diffraction (XRD), micro-Raman (MR) spectroscopy, field emission scanning electron microscopy (FE-SEM), and photoluminescence (PL) measurements. Our study revealed that the LNO layer contributed to the enhancement of the optical properties exhibited by the MTO film; that is, it led to unexpected behavior. Hence, computational simulation was performed by using the density functional theory (DFT) to gain a better understanding of the composition–structure–property relationships and reveal changes in the electronic structure properties of these thin films. These changes occurred mainly at the interface between the LNO/Si, MTO/Si, and MTO/LNO/Si structures, and were in good agreement with our experimental findings. Thus, we found that the PL properties of the nanostructured films were strongly dependent on their interface features.

## 2. RESULTS AND DISCUSSION

Figure 2 shows the XRD patterns of the as-prepared MTO/Si, LNO/Si, and MTO/LNO/Si nanostructured films. All samples were crystallized, and a long-range structural organization was revealed. The XRD patterns of the LNO/Si film (Figure 2a) revealed polycrystalline growth (without a preferred orientation) and the corresponding diffraction peaks were indexed in the rhombohedral structure with the  $R\bar{3}c$  space group by Card No. 00-033-0711 of the Joint Committee on Powder Diffraction Standards (JCPDS). For the MTO/Si film (Figure 2b), the corresponding diffraction peaks were also indexed in the rhombohedral structure with the  $R\bar{3}$  space group by JCPDS Card No. 01-079-0831. It was observed that the MTO/Si film exhibited a preferential orientation along the (003) direction. These results are consistent with previous works reported in the literature.<sup>18</sup> The MTO/LNO/Si heterostructure (Figure 2c) had a polycrystalline nature and exhibited well-defined diffraction peaks for both the MTO and LNO phases. This is in good agreement with JCPDS Card Nos. 01-079-0831 and 00-033-0711. Panels a and b of Figure 1 contain a schematic representation of the crystallographic unit cell of both MTO and LNO materials and its metal–oxygen polyhedra. The MTO structure exhibited unique face-shared and edge-shared

configurations for both the octahedral  $[\text{MgO}_6]$  and  $[\text{TiO}_6]$  clusters with a local symmetry ( $C_1$ ). In the LNO corundum structure, the octahedral  $[\text{NiO}_6]$  clusters had a  $C_1$  local symmetry, and the coordination polyhedra  $[\text{NiO}_6]$ - $[\text{NiO}_6]$  were linked at the corner and shared the face with the coordination complex  $[\text{LaO}_{12}]$  clusters ( $C_2$  point group). Additionally, due to the interfacial changes, the XRD patterns also reveal a shift to higher angles, indicating a significant increase in the lattice parameters and, therefore, most likely, strain formation during the lattice expansion. From a practical standpoint, chemical insights from defect engineering may provide essential clues for improving the synthetic methods and understanding fundamental nanoscale properties, driving innovation in the field of crystalline materials. Moreover, characteristic impurity peaks were not observed for any sample.

In this case, the MR measurements were employed to gain insights into the short-range structural order of these nanostructured films. Figure 3a shows the room temperature MR spectra of the MTO/Si, LNO/Si, and MTO/LNO/Si thin films. The Raman-active mode was found in all samples at approximately  $520\text{ cm}^{-1}$  and originated from the Si(100) substrate. According to group theory, the LNO phase with a rhombohedral structure belongs to the  $R\bar{3}c$  space group and has 27 optical modes, but only five are Raman-active modes (e.g.,  $A_{1g} + 4E_g$ ).<sup>19,20</sup> We experimentally observed four Raman-active modes for the LNO thin film at approximately 148 ( $E_g$ ), 203 ( $A_{1g}$ ), 397 ( $E_g$ ), and  $443\text{ cm}^{-1}$  ( $E_g$ ), as can be seen in Figure 3a. According to Chaban et al.,<sup>20</sup> the  $A_{1g}$  mode is a soft mode driving the structural distortion in the  $R\bar{3}c$  perovskites. The Raman-active mode located at  $148\text{ cm}^{-1}$  can be described as pure La vibrations along the  $a$ - and  $b$ -axes of the structure in the hexagonal  $\{001\}$ -plane.<sup>19</sup> Moreover, the Raman-active modes located at 397 and  $443\text{ cm}^{-1}$  were caused by the vibrational modes of the oxygen cage.<sup>20</sup>

However, it can be seen from Figure 3a that the MTO thin film had ten Raman-active modes (e.g.,  $5A_g + 5E_g$ ), as predicted in the literature.<sup>21–27</sup> This was attributed to high crystallization at short range. The  $A_g$  modes situated at 227 and  $300\text{ cm}^{-1}$  are mainly attributed to the vibrations of Mg and Ti atoms along the  $z$ -axis.<sup>25</sup> The other  $A_g$  modes observed at approximately 390, 500, and  $708\text{ cm}^{-1}$  are related to the breathing-like vibrations of the six O atoms. However, by comparing the modes, it can be seen that they had different vibration directions in the octahedral configuration.<sup>25,26</sup> The  $E_g$  mode typically observed at  $275\text{ cm}^{-1}$

is attributed to the antisymmetric breathing vibration of the O octahedron.<sup>25–27</sup> As shown in Figure 3a, the  $E_g$  modes located at 320, 344, and 480  $\text{cm}^{-1}$  can be described as the antisymmetric breathing and twisting vibrations of the O octahedron with the cationic vibrations of both the Mg and Ti atoms parallel to the XY-plane,<sup>22,26</sup> while the mode observed at approximately 620  $\text{cm}^{-1}$  is likely associated with the Ti–O stretch.<sup>22</sup> Moreover, the MR spectrum of the polycrystalline MTO/LNO/Si heterostructure (Figure 3a) exhibited all modes of both the MTO and LNO rhombohedral structures, which indicates that this sample prepared by the PLD method was structurally ordered at the short range. From these results, it is also noted that MR spectra have two asymmetric bands with the maximum centered at approximately 215 and 395  $\text{cm}^{-1}$ , respectively. Hence, the MR spectra were deconvoluted (after using the Bose–Einstein correction) from using multiple Lorentz functions, as shown in Figures 3b,c.<sup>28,29</sup> These bands are probably formed from an overlap of the vibrational modes of both MTO (214 and 390  $\text{cm}^{-1}$ ) and LNO (203 and 397  $\text{cm}^{-1}$ ) materials. As can be observed by the deconvolution, the vibrational mode  $A_g$  referring to the pure MTO is shifted to smaller Raman-active mode lengths (from 227 to 214  $\text{cm}^{-1}$ ) in the multilayer film, indicating that the interaction with the LNO causes a short-range lattice ordering.<sup>19–27</sup>

Figure 4 shows the FE-SEM micrographs of the surface microstructure and cross-section of the LNO/Si, MTO/Si, and

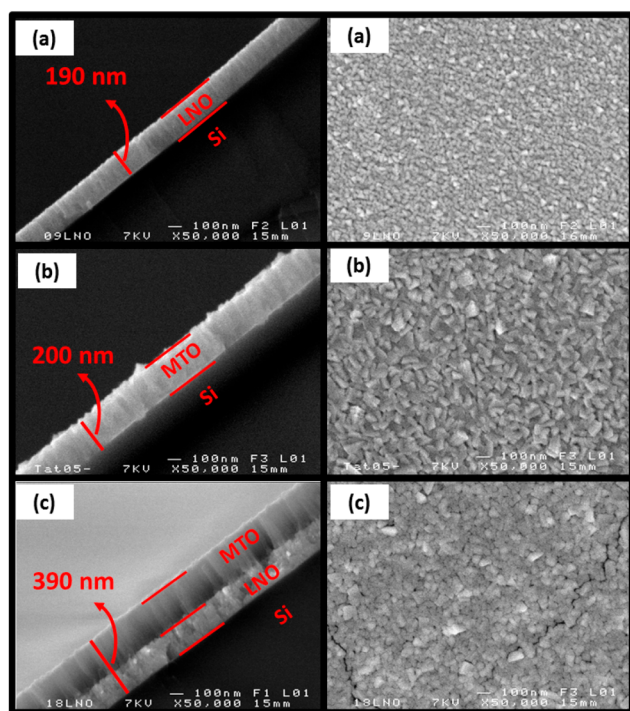


**Figure 4.** FE-SEM micrographs of the surface microstructure and cross-section of (a) LNO/Si, (b) MTO/Si, and (c) MTO/LNO/Si thin films.

MTO/LNO/Si thin films. As can be seen, the average thicknesses were 190, 200, and 390 nm for the LNO/Si, MTO/Si, and LNO/MTO/Si films, respectively. These values were deduced from the cross-section views and are in agreement with the deposition conditions used in this study. However, the FE-SEM micrographs revealed different grain microstructures for these thin films, i.e., suggesting a possible effect of the

different crystalline orientations for these polycrystalline materials due to interfacial changes previously discussed. In this case, the LNO/Si thin film is composed of more or less spherical grains, while the grains of the MTO/Si film are hexagon-shaped grains (i.e., related to the *c*-plane arrangement of the rhombohedral crystal structure).<sup>18</sup> Moreover, all of the deposited films had a dense microstructure with excellent contact interfaces (see cross-section views in Figure 4a–c), which is promising for developing various interesting technological applications.

It is important to note that a deeper understanding of the interface features is crucial when designing novel functional materials with tuned properties.<sup>30–34</sup> In this context, PL emission measurements combined with high-level DFT calculations are often employed to probe the effect of small changes in a crystalline structure. Hence, they can be easily used to reveal the critical role of these nanostructured films' interface features and provide essential clues for an in-depth understanding of their physical and chemical properties at the nanoscale.<sup>2,33–37</sup>

First, we investigated the PL emission spectra of the Si substrate, LNO/Si, MTO/Si, and MTO/LNO/Si nanostructured films, respectively, as shown in Figure 5b. These nanostructured films have a characteristic broadband PL emission. In this regard, it is well-known that the symmetry-breaking process can induce a robust structural polarization that leads to a nonhomogeneous charge distribution in these materials. This fact is closely associated with the structural order–disorder effects generated during the fabrication process,<sup>34</sup> which leads to a broadband PL emission for these systems (Figure 5b). A magnified view of the broadband PL emission profile of the Si substrate and LNO/Si suggests that these materials are structurally ordered at the medium range (see Supporting Information Figure S1).

The PL emission profile clearly indicates a weak broad luminescence for the Si substrate and LNO/Si, while much higher PL emissions were observed for MTO/Si and MTO/LNO/Si. This result revealed that the Si substrate had a low defect density at the medium range, in addition to revealing its “non-innocent” behavior, that is, the fact that the substrate plays a key role in the structural modification processes at the film/substrate interface. Hence, the Si substrate enables the formation control of the films' complex interface defects. This is extremely important to better understand the impact and synergistic effects of the complex interface defects responsible for modulating the optical properties of these novel functional materials.

The LNO/Si film indicated that the complex interface defects, which are a necessary condition to exhibit an intense PL emission, virtually cancel out the PL emission of these two materials. Thus, we concluded that LNO/Si had a low defect density at the film/substrate interface at medium range and that the behavior exhibited by these materials was mainly caused by structural defects (i.e., shallow defects). In contrast, for the MTO/Si film, we observed the most intense broad luminescence centered at 724 nm, in the near-infrared region. Also, the strong PL emission (in the near-infrared region) may also be related to the crystal orientation for these MTO/Si films as-prepared.<sup>18</sup> As a consequence, these findings are commonly consistent with our XRD results for MTO/Si films. Generally, this can be attributed to the chemical nature of the reactive species involved, and it is also strongly dependent on the experimental conditions used during the growth of such

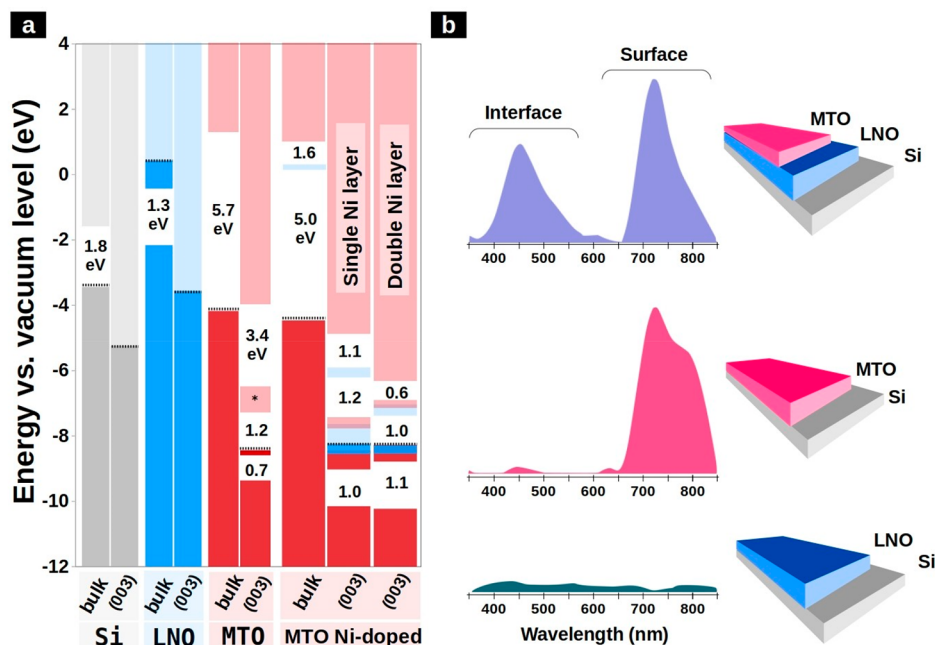


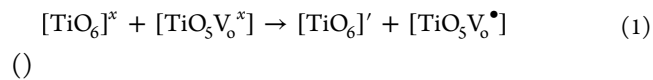
**Figure 5.** (a) Band diagram of Si, LNO, and MTO in both bulk and surface structures. The Ni-doped bulk and Ni-doped MTO (003) thin films band diagram showed midgap states related to Ni 3d filled and/or empty states. The horizontal dotted black line points out the Fermi level. The star on the midgap state of undoped MTO film is related to the triplet state (more stable than singlet one) and is absent on the singlet spin state. (b) PL spectra of LNO/Si, MTO/Si, and MTO/LNO/Si nanostructured films, excited with a 350.7 nm line of krypton ion laser.

films.<sup>34–37</sup> Therefore, these results suggest that the structural changes promoted particularly at the LNO/Si interface, in principle, reduce the polarization, which is capable of populating stable excited electronic states.<sup>38,39</sup> This interface phenomenon occurs at the short and medium ranges.

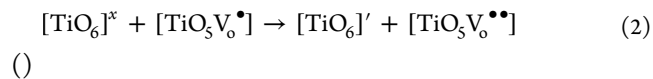
Interestingly, there was a visible change in the PL emission behavior for the MTO/LNO/Si interfaces. In particular, the PL emission profile of MTO/LNO/Si exhibited, for the first time, two intense broadband PL emissions with the maximum values centered at 454 nm (blue region) and 754 nm (near-infrared region), respectively. Therefore, on the basis of these results, it can be concluded that the interfacial change leads to the formation of new defect states and is the most probable cause for the appearance of PL peak at approximately 454 nm. Hence, the results provide evidence for the emergence of the first PL band emission, which can easily be attributed to the significantly high concentration of shallow defect states formed in the LNO layer, and particularly in the vicinity of the contact interface with the MTO layer, during the deposition of this one. Moreover, it should also be noted that the PL band emission observed at approximately 754 nm was significantly modified in comparison with the PL data for the MTO/Si (Figure 5b), mainly owing to the effects of the LNO layer, which in turn altered the structural characteristics of the MTO layer at the medium range. These findings provide solid evidence that the growth orientation of this MTO layer on the LNO leads to an increase of complex defects formed, especially at the interface region of this polycrystalline material, resulting in the emergence of entirely new properties. It is well-known that during the excitation process of such nanostructured films, the trapping of the electron–hole pairs occurs in the structural defects. In other words, the process is characterized by the involvement of numerous states within the band gap of the system as a result of the relaxation,<sup>26,33–38</sup> and an intense emission of the photon also occurs.<sup>26,33–38</sup> Our results revealed that the PL emission

behavior of these novel high-quality functional materials is, in turn, actively controlled by their interface features. Also, the multipeak fitting of PL spectra was performed using the Voigt function and are presented in Supporting Information Figure S2.

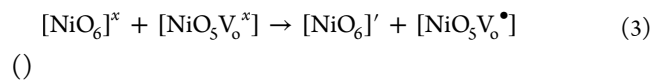
Clearly, the above-mentioned important underlying physical behavior can be easily explained from a structural perspective. Thus, the different intrinsic (hence the bulk surface) and extrinsic (hence the contact interface) defect distributions play a crucial role in streamlining the behavior of the PL emissions at the nanoscale.<sup>33–35,38</sup> To clarify the small structural changes that occur mainly at the contact interface of these nanostructured films, we elucidate the cluster-to-cluster charge transfer processes (CCCT) based on the cluster complex notation of such systems,<sup>36</sup> as follows:



()



()



()



() where both the  $[\text{TiO}_6]$  and  $[\text{NiO}_6]$  clusters are donors, the  $[\text{TiO}_5\text{VO}^\bullet]$  and  $[\text{NiO}_5\text{VO}^\bullet]$  clusters are donors–acceptors, and the  $[\text{TiO}_5\text{VO}^{\bullet\bullet}]$  and  $[\text{NiO}_5\text{VO}^{\bullet\bullet}]$  clusters are acceptors. According to the structural analysis, the effect of the surface and/or interface properties on the PL performance should be considered in terms of  $[\text{TiO}_6]_o^x$  and  $[\text{NiO}_6]_o^x$  clusters, and  $[\text{TiO}_5\text{V}_o^x]_d$  and  $[\text{NiO}_5\text{V}_o^x]_d$  clusters, where o = order and d = disorder. By following the above logic, an effective charge separation (i.e., electron–hole) requires the presence of a CCCT process,<sup>26,33</sup> which occurs particularly in the interface

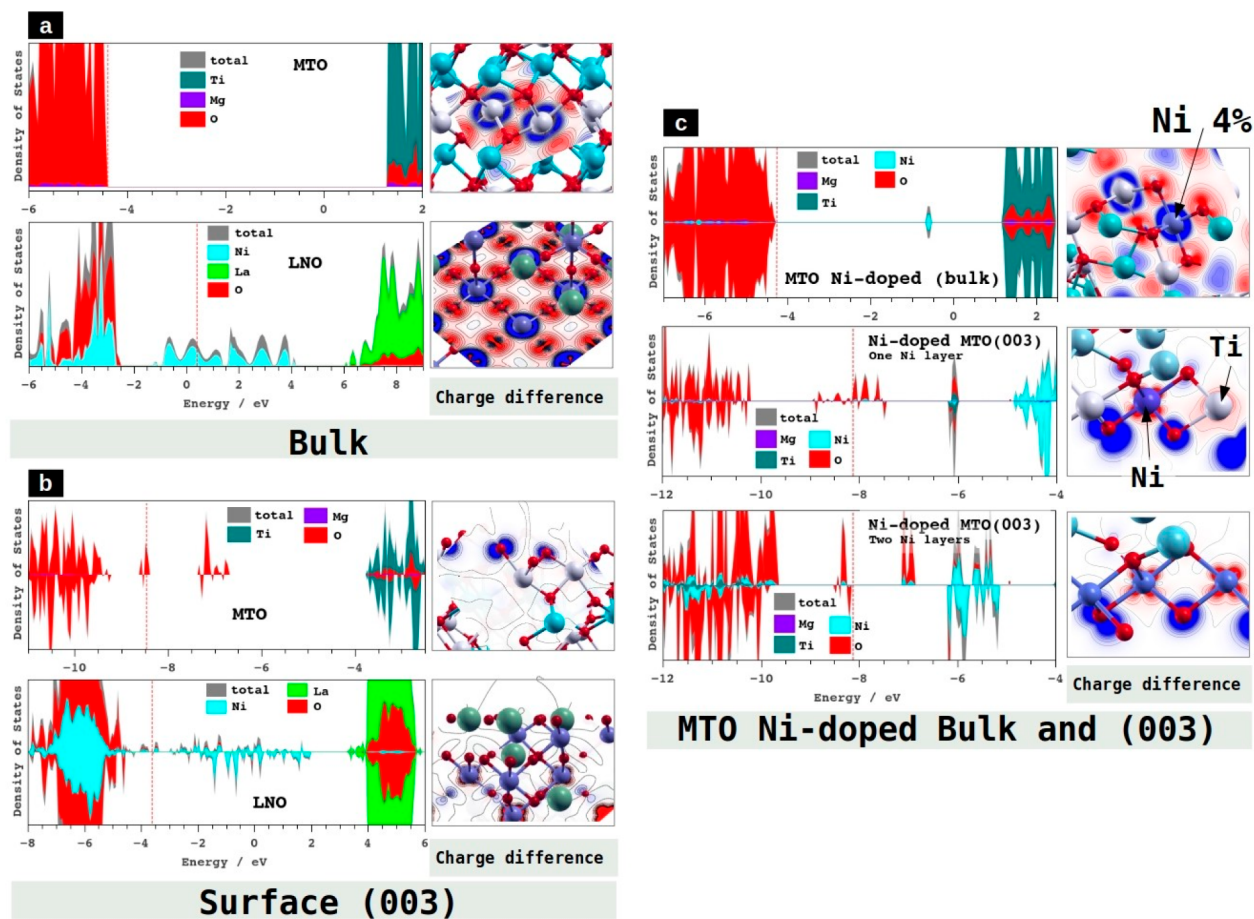
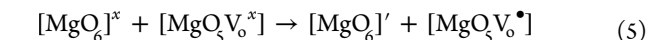
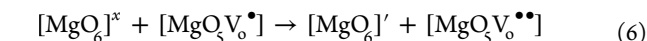


**Figure 6.** Total and projected DOS of (a) MTO and LNO in bulk phases, (b) MTO and LNO in the (003) thin films, and (c) Ni-doped MTO bulk and (003) thin film.

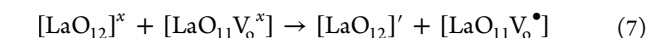
region of such thin films. Hence, the CCCT process likely involves the formation and recombination of all complex clusters from  $[\text{TiO}_6]_o^x/[\text{TiO}_5\text{V}_o^x]_d$ ,  $[\text{NiO}_6]_o^x/[\text{NiO}_5\text{V}_o^x]_d$ ,  $[\text{NiO}_5\text{V}_o^x]_d/[\text{TiO}_5\text{V}_o^x]_d$ , and  $[\text{NiO}_6]_o^x/[\text{TiO}_5\text{V}_o^x]_d$ . Additionally, this model can, in principle, be extended for the lattice modifiers. In this case, the charge will transfer from  $[\text{TiO}_6]$  to  $[\text{MgO}_6]^x$  or from  $[\text{NiO}_6]$  to  $[\text{LaO}_9]^x/[\text{CuO}_{12}]_d$  and from  $[\text{MgO}_5\text{V}_o^z]$  to  $[\text{MgO}_6]^x$  or from  $[\text{LaO}_{11}\text{V}_o^z]$  to  $[\text{LaO}_{12}]^x$ , as expressed by the following equations:



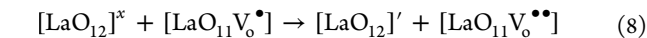
( )



( )



( )



( )

In short, we have provided a full structural description to clarify the optical behavior of these nanostructured films. Moreover, this description will allow us to quickly identify two effects that are generally responsible for modulating the PL emission of such materials. Remarkably, the first effect can be attributed to the intrinsic defects in the Si, LNO, or MTO materials, i.e., the defects derived from the material constituted

by the oxygen vacancies in three different charge states ( $\text{V}_o^z = \text{V}_o^x, \text{V}_o^\bullet, \text{or } \text{V}_o^{\bullet\bullet}$ ), which allow for the excited  $[\text{SiO}_3\text{V}_o^z]$ ,  $[\text{LaO}_{11}\text{V}_o^z]$ ,  $[\text{NiO}_5\text{V}_o^z]$ ,  $[\text{MgO}_5\text{V}_o^z]$ , and  $[\text{TiO}_5\text{V}_o^z]$  clusters. The second effect typically results from the interface features between these complex clusters, which produce extrinsic defects by combining and interacting, which in turn decrease or increase the band gap, and hence can either allow the PL emission or not. Moreover, before the photon arrival, the short- and medium-range structural defects, in particular, generate localized states within the band gap and a nonhomogeneous charge distribution in the unit cell.<sup>26,34–38</sup> After the photon arrival, the lattice configuration changes. Additionally, distorted excited clusters are formed and allow electrons to become trapped.<sup>36,37</sup> In the latter, it is well-known that the photons decay by radiative or nonradiative relaxations.

Additionally, the effect of band alignment on the optical behavior of these nanostructured films was investigated. When the band structures of the Si, MTO, and LNO surfaces are placed side by side, the Fermi level of MTO has a lower value (Figure 5a). Generally, the distortion on the surfaces and around the interfaces should modify the complex clusters and their effective coordination number that originate mainly from the spin reorientation in these clusters and lead to electron clustering and hole formation. Moreover, the band alignment of the novel MTO/LNO/Si nanostructured films revealed the decisive role of the interface complex defects in the control of their remarkable properties: the electrons transferred from the

MTO to Si, while the holes transferred from Si to MTO (Figure 5a).

Notably, the modulation of the strain during the growth of thin films on diverse substrates has a tremendous impact on their fundamental properties and is extremely interesting from the technological standpoint.<sup>40–42</sup> Overall, it is well-known that the substrate has a considerable influence on the structural quality of the prepared thin film.<sup>40</sup> These results, however, reveal that, despite the similar thickness, the crystalline structure qualities of the MTO film grown on Si substrate and those on the LNO layer are very different in terms of the distribution of complex defects. This indicates that some parts of the interface can, in principle, exhibit different crystalline orientations, which are fundamental to understanding this phenomenon. Hence, as a consequence, this region is more likely to exhibit a greater density of defects, as well as have a significant influence on the kind of surface grown, and still can have a descending role in phase control.<sup>40–42</sup> To gain further insights, we calculated the total and atom-resolved DOS projected for both the bulk and (003) surfaces, as shown in Figure 5.

Silicon bulk is a well-known semiconductor with a low band gap.<sup>39</sup> However, its (003) surface is a conductor because of the outermost Si with low coordination (see Supporting Information Figure S3). Additionally, LNO is the conductor in both models, mainly because of the partially filled Ni 3d states. In particular, the LNO (003) surface is ferromagnetic, as shown in the DOS and spin density map (Figure 6). Its Fermi level is higher than that of Si (003). However, the electronic structure of MTO is entirely different. The MTO bulk is a semiconductor with a band gap of approximately 5.7 eV, where the edges of the valence and conduction bands (denoted as VB and CB, respectively) are composed mostly of O 2p and Ti 3d states, respectively. The MTO (003) surface exhibits occupied and empty midgap states located on the low coordinated oxygen at the outmost layers of the surface. Overall, these results provide two spin configuration solutions for the (003) MTO thin film, as shown in Figure 5: a ground singlet state ( $S_0$ ) and the most stable ( $\sim 0.7$  eV) triplet ( $T_1$ ) configuration. The spin density of that intermediary level is shown in Figure 6. Consequently, the main difference between them is the Ti 3d empty midgap state located 1.2 eV above the VB, as shown in Figure 6. This state is absent in the singlet MTO film and may be a channel for electronic excitation and recombination of photogenerated excitons.<sup>43,44</sup> This midgap state is 3.4 eV below the next CB, also composed by empty Ti 3d and O 2p states. Hence, the effect of isolated Ni on MTO bulk, at approximately 4% Ni to Ti substitution, introduced an empty midgap state of Ni 3d, 1.6 eV below the CB. Compared with the pristine MTO bulk, the band gap was significantly reduced from 5.7 to 5.0 eV within the doping model used in this study. Despite the high value of the theoretical band gap, in general, it is necessary to focus only on the difference (or relative values) of band gaps, because of the errors and limitations well-known for the exchange–correlation functionals. The presented model was taken as a limiting situation. Because it is more probable that there is a high concentration of defects in the interface of the polycrystalline films, this could lead to a possible reduction in the diffusion of isolated cations. In fact, this is consistent with the experimental measurements and conditions used in the PLD deposition. However, even so, one still cannot wholly exclude this possibility. Based on this premise, two situations of Ni doping on (003) MTO thin films were checked: (i) Ni sharing the first and second metal layers with Ti on MTO thin films and (ii) Ni

occupying the first two metal layers. In the first case, the system is a conductor, whereas, in the second, the filled and empty Ni 3d and Ti 3d states are separated by 1.0 eV. Figure 6 showed the density charge maps for these models. In this case, the oxygens coordinated with those metals can display a pivotal role in the interpretation of this physical phenomenon. Therefore, these results can be easily elucidated from a modern structural perspective based on complex cluster modeling. This revealed the structural order–disorder effects (i.e., at the short, medium, and long ranges) on the physical and chemical properties of the novel MTO/LNO/Si nanostructured films and their interface features at the nanoscale. It is widely known that these cluster complexes are strongly dependent on the synthesis methods and conditions.<sup>33,38</sup>

### 3. CONCLUSION

In summary, MTO/Si, LNO/Si, and MTO/LNO/Si thin films with a rhombohedral crystalline structure were successfully obtained by the PLD method and structurally ordered at the short and long ranges. The MTO/Si thin film exhibited a (003) orientation, whereas the LNO/Si thin film was polycrystalline. Both polycrystalline LNO and MTO phases were obtained in the MTO/LNO/Si multilayer film. The FE-SEM micrographs revealed an excellent contact interface for such densely structured thin films. However, the PL emission behavior is probably related to a structural disorder at the medium range. Hence, the PL mechanism for these thin films can be easily explained from a structural perspective. Our theoretical and experimental findings clarified the role of small structural changes occurring mainly in the interface region of these thin films and leading to the control of unexpected PL emission behavior. These results also revealed a complex relationship between the structure and the properties at nanoscale, which opens up novel application opportunities for these films in a variety of emerging optoelectronic technologies.

### ■ ASSOCIATED CONTENT

#### Supporting Information

The Supporting Information is available free of charge on the ACS Publications website at DOI: 10.1021/acsanm.8b02110.

Experimental section, including sample preparation, characterizations, theoretical models and methods, and optical results and DOS of Si bulk and (003) thin film (PDF)

### ■ AUTHOR INFORMATION

#### Corresponding Author

\*E-mail: felipe\_laporta@yahoo.com.br; felipelaporta@utfpr.edu.br.

#### ORCID

L. F. Gorup: 0000-0003-2646-8026

A. R. Albuquerque: 0000-0001-7727-266X

J. R. Sambrano: 0000-0002-5217-7145

F. A. La Porta: 0000-0003-0990-7947

E. Longo: 0000-0001-8062-7791

#### Notes

The authors declare no competing financial interest.

### ■ ACKNOWLEDGMENTS

The financial support from the CNPq (Grant 159387/2015-9), FAPESP (Grant 2013/07296-2), and CAPES is gratefully

acknowledged. We are grateful for the assistance in SEM observations of the staff of the CMEBA facility (ScanMAT, UMS 2001 CNRS—University of Rennes 1) which received financial support from the Région Bretagne and European Union (CPER-FEDER 2007–2014, Présage No. 39126 and Présage No. 37339).

## REFERENCES

- (1) Okada, T.; Narita, T.; Nagai, T.; Yamanaka, T. Comparative Raman spectroscopic study on ilmenite-type  $\text{MgSiO}_3$  (akimotoite),  $\text{MgGeO}_3$ , and  $\text{MgTiO}_3$  (geikielite) at high temperatures and high pressures. *Am. Mineral.* **2008**, *93*, 39–47.
- (2) Hwang, H. Y.; Iwasa, Y.; Kawasaki, M.; Keimer, B.; Nagaosa, N.; Tokura, Y. Emergent phenomena at oxide interfaces. *Nat. Mater.* **2012**, *11*, 103–113.
- (3) Linton, J. A.; Fei, Y. W.; Navrotsky, A. The  $\text{MgTiO}_3$ – $\text{FeTiO}_3$  join at high pressure and temperature. *Am. Mineral.* **1999**, *84*, 1595.
- (4) Ferreira, V. M.; Baptista, J. L.; Petzelt, J.; Komandin, G. A.; Voitsekhovskii, V. V. Loss spectra of pure and La-doped  $\text{MgTiO}_3$  microwave ceramics. *J. Mater. Res.* **1995**, *10*, 2301–2305.
- (5) Alves, M. C. F.; Boursicot, S.; Ollivier, S.; Bouquet, V.; Députier, S.; Perrin, A.; Weber, I. T.; Souza, A. G.; Santos, I. M. G.; Guilloux-Viry, M. Synthesis of  $\text{SrSnO}_3$  thin films by pulsed laser deposition: Influence of substrate and deposition temperature. *Thin Solid Films* **2010**, *519*, 614–618.
- (6) Le Febvrier, A.; Députier, S.; Bouquet, V.; Demange, V.; Ollivier, S.; Galca, A. C.; Dragoi, C.; Radu, R.; Pintilie, L.; Guilloux-Viry, M. Ferroelectric and dielectric multilayer heterostructures based on  $\text{KTa}_{0.65}\text{Nb}_{0.35}\text{O}_3$  and  $\text{Bi}_{1.5-x}\text{Zn}_{0.92-y}\text{Nb}_{1.5}\text{O}_{6.92-1.5x-y}$  grown by pulsed laser deposition and chemical solution deposition for high frequency tunable devices. *Thin Solid Films* **2012**, *520*, 4564–4567.
- (7) Kalabukhov, A.; Boikov, Y. A.; Serenkov, I. T.; Sakharov, V. I.; Börjesson, J.; Ljustina, N.; Olsson, E.; Winkler, D.; Claesson, T. Improved cationic stoichiometry and insulating behavior at the interface of  $\text{LaAlO}_3/\text{SrTiO}_3$  formed at high oxygen pressure during pulsed-laser deposition. *Europhys. Lett.* **2011**, *93*, 37001.
- (8) Cichetto, L., Jr; Sergeenkov, S.; Diaz, J. C. C. A.; Longo, E.; Araújo-Moreira, F. M. Influence of substrate on structural and transport properties of  $\text{LaNiO}_3$  thin films prepared by pulsed laser deposition. *AIP Adv.* **2017**, *7*, No. 025005.
- (9) Fujioka, Y.; Frantti, J.; Rouleau, C.; Puretzy, A.; Meyer, H. M. Vacancy filled nickel-cobalt-titanate thin films. *Phys. Status Solidi B* **2017**, *254*, 1600799.
- (10) Hu, D.; Ma, H.; Tanaka, Y.; Zhao, L.; Feng, Q. Ferroelectric Mesocrystalline  $\text{BaTiO}_3/\text{SrTiO}_3$  Nanocomposites with Enhanced Dielectric and Piezoelectric Responses. *Chem. Mater.* **2015**, *27*, 4983–4994.
- (11) Li, J.; Yin, D.; Li, Q.; Sun, R.; Huang, S.; Meng, F. Interfacial defects induced electronic property transformation at perovskite  $\text{SrVO}_3/\text{SrTiO}_3$  and  $\text{LaCrO}_3/\text{SrTiO}_3$  heterointerfaces. *Phys. Chem. Chem. Phys.* **2017**, *19*, 6945–6951.
- (12) Lemée, N.; Infante, I. C.; Hubault, C.; Boule, A.; Blanc, N.; Boudet, N.; Demange, V.; Karkut, M. G. Polarization Rotation in Ferroelectric Tricolor  $\text{PbTiO}_3/\text{SrTiO}_3/\text{PbZr}_{0.2}\text{Ti}_{0.8}\text{O}_3$  Superlattices. *ACS Appl. Mater. Interfaces* **2015**, *7*, 19906–19913.
- (13) Belnou, F.; Bernard, J.; Houivet, D.; Haussonne, J. M. Low temperature sintering of  $\text{MgTiO}_3$  with bismuth oxide based additions. *J. Eur. Ceram. Soc.* **2005**, *25*, 2785–2789.
- (14) Miao, Y.-M.; Zhang, Q.-L.; Yang, H.; Wang, H.-P. Low-temperature synthesis of nano-crystalline magnesium titanate materials by the sol–gel method. *Mater. Sci. Eng., B* **2006**, *128*, 103–106.
- (15) Zhang, W. F.; Yin, Z.; Zhang, M. S.; Du, Z. L.; Chen, W. C. Roles of defects and grain sizes in photoluminescence of nanocrystalline  $\text{SrTiO}_3$ . *J. Phys.: Condens. Matter* **1999**, *11*, S655.
- (16) Leonelli, R.; Brebner, J. L. Growth of  $\text{InGaAsP}$  distributed feedback lasers by a modified single-phase LPE technique. *Solid State Commun.* **1985**, *54*, 505–507.
- (17) Ferri, E. A. V.; Mazzo, T. M.; Longo, V. M.; Moraes, E.; Pizani, P. S.; Li, M. S.; Espinosa, J. W. M.; Varela, J. A.; Longo, E. Very Intense Distinct Blue and Red Photoluminescence Emission in  $\text{MgTiO}_3$  Thin Films Prepared by the Polymeric Precursor Method: An Experimental and Theoretical Approach. *J. Phys. Chem. C* **2012**, *116*, 15557–15567.
- (18) Ho, Y. D.; Huang, C. L. Strong Near-Infrared Photoluminescence Emission of (003)-Oriented  $\text{MgTiO}_3$  Thin Films. *J. Am. Ceram. Soc.* **2013**, *96*, 2065–2068.
- (19) Hsiao, C. Y.; Shih, C. F.; Chien, C. H.; Huang, C. L. Textured Magnesium Titanate as Gate Oxide for GaN-Based Metal-Oxide-Semiconductor Capacitor. *J. Am. Ceram. Soc.* **2011**, *94*, 363.
- (20) Chaban, N.; Weber, M.; Pignard, S.; Kreisel, J. Phonon Raman scattering of perovskite  $\text{LaNiO}_3$  thin films. *Appl. Phys. Lett.* **2010**, *97*, No. 031915.
- (21) Abrashev, M. V.; Litvinchuk, A. P.; Iliev, M. N.; Meng, R. L.; Popov, V. N.; Ivanov, V. G.; Chakalov, R. A.; Thomsen, C. Comparative study of optical phonons in the rhombohedrally distorted perovskites  $\text{LaAlO}_3$  and  $\text{LaMnO}_3$ . *Phys. Rev. B: Condens. Matter Mater. Phys.* **1999**, *59*, 4146.
- (22) Wang, C. H.; Jing, X. P.; Feng, W.; Lu, J. Assignment of Raman-active vibrational modes of  $\text{MgTiO}_3$ . *J. Appl. Phys.* **2008**, *104*, No. 034112.
- (23) Reynard, B.; Guyot, F. High-temperature properties of geikielite ( $\text{MgTiO}_3$ -ilmenite) from high-temperature high-pressure Raman spectroscopy - Some implications for  $\text{MgSiO}_3$ -ilmenite. *Phys. Chem. Miner.* **1994**, *21*, 441–450.
- (24) Hirata, T.; Ishioka, K.; Kitajima, M. J. Vibrational Spectroscopy and X-Ray Diffraction of Perovskite Compounds  $\text{Sr}_{1-x}\text{M}_x\text{TiO}_3$  ( $\text{M} = \text{Ca}, \text{Mg}; 0 < x < 1$ ). *J. Solid State Chem.* **1996**, *124*, 353–359.
- (25) Ferri, E. A. V.; Sczancoski, J. C.; Cavalcante, L. S.; Paris, E. C.; Espinosa, J. W. M.; de Figueiredo, A. T.; Pizani, P. S.; Mastelaro, V. R.; Varela, J. A.; Longo, E. Photoluminescence behavior in  $\text{MgTiO}_3$  powders with vacancy/distorted clusters and octahedral tilting. *Mater. Chem. Phys.* **2009**, *117*, 192–198.
- (26) Nakata, M. M.; Mazzo, T. M.; Casali, G. P.; La Porta, F. A.; Longo, E. A large red-shift in the photoluminescence emission of  $\text{Mg}_{1-x}\text{Sr}_x\text{TiO}_3$ . *Chem. Phys. Lett.* **2015**, *622*, 9–14.
- (27) Filipović, S.; Obradović, N.; Pavlović, V. B.; Mitrić, M.; Đorđević, A.; Kachlik, M.; Maca, K. Effect of consolidation parameters on structural, microstructural and electrical properties of magnesium titanate ceramics. *Ceram. Int.* **2016**, *42*, 9887–9898.
- (28) Venimadhav, A.; Yates, K. A.; Blamire, M. G. Scanning Raman Spectroscopy for Characterizing Compositionally Spread Films. *J. Comb. Chem.* **2005**, *7*, 85–89.
- (29) Yoon, S.; Liu, H. L.; Schollerer, G.; Cooper, S. L.; Han, P. D.; Payne, D. A.; Cheong, S. W.; Fisk, Z. *Phys. Rev. B: Condens. Matter Mater. Phys.* **1998**, *58*, 2795.
- (30) Adhikari, S.; Garcia-Castro, A. C.; Romero, A. H.; Lee, H.; Lee, J. W.; Ryu, S.; Eom, C. B.; Cen, C. Charge Transfer to  $\text{LaAlO}_3/\text{SrTiO}_3$  Interfaces Controlled by Surface Water Adsorption and Proton Hopping. *Adv. Funct. Mater.* **2016**, *26*, 5453–5459.
- (31) Guerrero, A.; Garcia-Belmonte, G.; Mora-Sero, I.; Bisquert, J.; Kang, Y. S.; Jacobsson, T. J.; Correa-Baena, J. P.; Hagfeldt, A. Properties of Contact and Bulk Impedances in Hybrid Lead Halide Perovskite Solar Cells Including Inductive Loop Elements. *J. Phys. Chem. C* **2016**, *120*, 8023–8032.
- (32) Andres, J.; Gracia, L.; Gonzalez-Navarrete, P.; Longo, V. M.; Avansi, W.; Volanti, D. P.; Ferrer, M. M.; Lemos, P. S.; La Porta, F. A.; Hernandez, A. C.; Longo, E. Structural and electronic analysis of the atomic scale nucleation of Ag on  $\alpha\text{-Ag}_2\text{WO}_4$  induced by electron irradiation. *Sci. Rep.* **2015**, *4*, 5391.
- (33) Longo, E.; La Porta, F. d. A., Eds. *Recent Advances in Complex Functional Materials: From Design to Application*; Springer: Cham, Switzerland, 2017.
- (34) Oliveira, L. H.; Ramirez, M. A.; Ponce, M. A.; Ramajo, L. A.; Albuquerque, A. R.; Sambrano, J. R.; Longo, E.; Castro, M. S.; La Porta, F. A. Optical and gas-sensing properties, and electronic structure of the mixed-phase  $\text{CaCu}_3\text{Ti}_4\text{O}_{12}/\text{CaTiO}_3$  composites. *Mater. Res. Bull.* **2017**, *93*, 47–55.



(35) Longo, V. M.; Cavalcante, L. S.; Paris, E. C.; Sczancoski, J. C.; Pizani, P. S.; Li, M. S.; Andres, J.; Longo, E.; Varela, J. A. Hierarchical Assembly of CaMoO<sub>4</sub> Nano-Octahedrons and Their Photoluminescence Properties. *J. Phys. Chem. C* **2011**, *115*, 5207–5219.

(36) Gracia, L.; Longo, V. M.; Cavalcante, L. S.; Beltrán, A.; Avansi, W.; Li, M. S.; Mastelaro, V. R.; Varela, J. A.; Longo, E.; Andrés, J. Presence of excited electronic state in CaWO<sub>4</sub> crystals provoked by a tetrahedral distortion: An experimental and theoretical investigation. *J. Appl. Phys.* **2011**, *110*, No. 043501.

(37) Batista, F. M. C.; La Porta, F. A.; Gracia, L.; Cerdeiras, E.; Mestres, L.; Li, M. S.; Batista, N. C.; Andrés, J.; Longo, E.; Cavalcante, L. S. A joint experimental and theoretical study on the electronic structure and photoluminescence properties of Al<sub>2</sub>(WO<sub>4</sub>)<sub>3</sub> powders. *J. Mol. Struct.* **2015**, *1081*, 381–388.

(38) Silva Junior, E.; La Porta, F. A.; Liu, M. S.; Andrés, J.; Varela, J. A.; Longo, E. A relationship between structural and electronic order–disorder effects and optical properties in crystalline TiO<sub>2</sub> nanomaterials. *Dalton Trans.* **2015**, *44*, 3159–3175.

(39) Guo, Y.; Wang, Q.; Kawazoe, Y.; Jena, P. A New Silicon Phase with Direct Band Gap and Novel Optoelectronic Properties. *Sci. Rep.* **2015**, *5*, 14342.

(40) Schlom, D. G.; Chen, L.-Q.; Eom, C.-B.; Rabe, K. M.; Streiffer, S. K.; Triscone, J.-M. Strain Tuning of Ferroelectric Thin Films. *Annu. Rev. Mater. Res.* **2007**, *37*, 589–626.

(41) Guo, H.; Zhao, R.; Jin, K.-J.; Gu, L.; Xiao, D.; Yang, Z.; Li, X.; Wang, L.; He, X.; Gu, J.; Wan, Q.; Wang, C.; Lu, H.; Ge, C.; He, M.; Yang, G. Interfacial-Strain-Induced Structural and Polarization Evolutions in Epitaxial Multiferroic BiFeO<sub>3</sub> (001) Thin Films. *ACS Appl. Mater. Interfaces* **2015**, *7*, 2944–2951.

(42) Phadnis, C.; Sonawane, K. G.; Hazarika, A.; Mahamuni, S. Strain-Induced Hierarchy of Energy Levels in CdS/ZnS Nanocrystals. *J. Phys. Chem. C* **2015**, *119*, 24165–24173.

(43) Chakrabarti, S.; Biswas, K. DFT study of Mg<sub>2</sub>TiO<sub>4</sub> and Ni doped Mg<sub>1.5</sub>Ni<sub>0.5</sub>TiO<sub>4</sub> as electrode material for Mg ion battery application. *J. Mater. Sci.* **2017**, *52*, 10972–10980.

(44) Klimov, V. I. Mechanisms for Photogeneration and Recombination of Multiexcitons in Semiconductor Nanocrystals: Implications for Lasing and Solar Energy Conversion. *J. Phys. Chem. B* **2006**, *110*, 16827–16845.